3-15-2017

Size Distributions of Coastal Ocean Suspended Particulate Inorganic Matter: Amorphous Silica and Clay Minerals and their Dynamics

Xiaodong Zhang
University of North Dakota, xiaodong.zhang2@UND.edu

Robert H. Stavn

Alexander U. Falster

Johannes J. Rick

Deric Gray

See next page for additional authors

Estuarine, Coastal and Shelf Science 189 (2017) 243–251

Contents lists available at ScienceDirect

Estuarine, Coastal and Shelf Science

journal homepage: www.elsevier.com/locate/ecss

Size distributions of coastal ocean suspended particulate inorganic matter: Amorphous silica and clay minerals and their dynamics

Xiaodong Zhang [a], Robert H. Stavn [b, *], Alexander U. Falster [c], Johannes J. Rick [d], Deric Gray [e], Richard W. Gould Jr. [f]

[a] Department of Earth System Science and Policy, University of North Dakota, Grand Forks, ND 58202-9011, USA
[b] US Naval Research Laboratory, Code 7330, Stennis Space Center, MS 39529, USA
[c] Maine Mineral and Gem Museum, Bethel, ME 04217, USA
[d] Alfred-Wegener-Institut Helmholtz-Zentrum für Polar- und Meeresforschung, Wadden Sea Station, List(Sylt), Germany
[e] US Naval Research Laboratory, Code 7231, Washington, DC 20375, USA
[f] US Naval Research Laboratory, Code 7331, Stennis Space Center, MS 39529, USA

ARTICLE INFO

Article history:
Received 19 October 2016
Received in revised form
5 March 2017
Accepted 13 March 2017
Available online 15 March 2017

ABSTRACT

Particulate inorganic matter (PIM) is a key component in estuarine and coastal systems and plays a critical role in trace metal cycling. Better understanding of coastal dynamics and biogeochemistry requires improved quantification of PIM in terms of its concentration, size distribution, and mineral species composition. The angular pattern of light scattering contains detailed information about the size and composition of particles. These volume scattering functions (VSFs) were measured in Mobile Bay, Alabama, USA, a dynamic, PIM dominated coastal environment. From measured VSFs, we determined through inversion the particle size distributions (PSDs) of major components of PIM, amorphous silica and clay minerals. An innovation here is the extension of our reported PSDs significantly into the submicron range. The PSDs of autochthonous amorphous silica exhibit two unique features: a peak centered at about 0.8 μm between 0.2 and 4 μm and a very broad shoulder essentially extending from 4 μm to >100 μm. With an active and steady particle source from blooming diatoms, the shapes of amorphous silica PSDs for sizes <10 μm varied little across the study area, but showed more particles of sizes >10 μm inside the bay, likely due to wind-induced resuspension of larger frustules that have settled. Compared to autochthonous amorphous silica, the allochthonous clay minerals are denser and exhibit relatively narrower PSDs with peaks located between 1 and 4 μm. Preferential settling of larger mineral particles as well as the smaller but denser illite component further narrowed the size distributions of clay minerals as they were being transported outside the bay. The derived PSDs also indicated a very dynamic situation in Mobile Bay when a cold weather front passed through during the experiment. With northerly winds of speeds up to 15 m s^{-1}, both amorphous silica and clay minerals showed a dramatic increase in concentration and broadening in size distribution outside the exit of the barrier islands, indicative of wind-induced resuspension and subsequent advection of particles out of Mobile Bay. While collectively recognized as the PIM, amorphous silica and clay minerals, as shown in this study, possess very different size distributions. Considering how differences in PSDs and the associated particle areas will effect differences in sorption/desorption properties of these components, the results also demonstrate the potential of applying VSF-inversion in studying biogeochemistry in the estuarine-coastal ocean system.

1. Introduction

Particulate inorganic matter (PIM) is a key component in estuarine and coastal systems. PIM includes different types of particles, such as biogenic amorphous silica and calcite, and minerogenic clay, with each behaving differently biogeochemically. Biogenic amorphous silica (opal) forms a critical link in the biogeochemical

* Corresponding author. Permanent address: Department of Biology, University of North Carolina at Greensboro, Greensboro, NC 27402, USA.
E-mail address: stavnr@uncg.edu (R.H. Stavn).

http://dx.doi.org/10.1016/j.ecss.2017.03.025

cycle of silica by transforming dissolved silicate to particulate material (DeMaster, 1981; Tréguer et al., 1995). Clay minerals, mainly land-derived, are a dominant component of most marine sediments (Griffin et al., 1968). Biogenic or non-biogenic, PIM is also very active in the adsorption of nutrients and trace elements (Le Pape et al., 2012; Schlegel et al., 2001; Warren and Zimmerman, 1994), and hence play a key role in carbon and nutrient cycles in estuaries, coasts, and continental shelves (Corbett et al., 2004). For example, clay minerals have been implicated in stimulating phytoplankton productivity by supplying their adsorbed iron (Johnson et al., 1999), phosphate (Effler et al., 2014; Howarth et al., 2011), or dissolved silicate (Fachini and Vasconcelos, 2005).

Better understanding of coastal dynamics and biogeochemistry requires improved quantification of PIM in terms of its concentration, size distribution, and mineral species composition. Advances in biogeo-optics have enabled partitioning optical properties among suspended minerals and the various compartments of suspended organic matter (Bowers and Binding, 2006; Duarte et al., 1998; Stavn and Richter, 2008). Recently developed optical inversions of the total volume scattering functions (VSFs) (Zhang et al., 2011, 2012) measured over various coastal waters yielded, for the first time, an expanded range of the particle size distributions (PSDs) to the submicron level, i.e. the colloidal range, for the separate inorganic and organic components of suspended matter (Zhang et al., 2014). The PSD pattern retrieved in Zhang et al. (2014) is consistent with the predicted shape by Risović (1993) in which the distribution of total particles is the result of summing individual particle PSDs that can be described as gamma or log-normal distributions and in which the numbers of submicron particles level off and eventually decline as the particles become smaller.

In this study, we report a refinement to the Zhang et al. (2014) study by further examining PIM in two subgroups, amorphous silica and clay minerals, which are known to have very different biogeochemical properties. For example, clay minerals have a strong affinity for metals (e.g., Cr, Mn, Fe, Zn of group one and Mo of group two) and dissolved organic matter primarily at the Al-OH bonds at the edges of clay lamellae (Tombácz et al., 2004; van der Weijden et al., 1997). Detrital diatom frustules, however, have very specific affinities through their micropores and Si-OH bonding on the amorphous silica matrix (Schmitt et al., 2001). It has also been demonstrated that living diatoms resist adsorption of foreign materials on the surface of the frustule (Kranck and Milligan, 1988). Furthermore, sorption-desorption affinities differ depending on the size class of the suspended mineral matter (Liang et al., 2011; Salomons and Mook, 1977; Ussher et al., 2013). The mass concentration and size distribution for each group are determined from the VSF-inversion method and validated by comparing with laboratory gravimetric determinations. We focus on a dynamic coastal area, Mobile Bay, Alabama, USA, particularly during a winter frontal event. The size distributions of amorphous silica and clay minerals differ significantly from each other due to differences in their origins and particle characteristics. The size distributions also change in response to wind-induced resuspension and subsequent advection of suspended particles. To the best of our knowledge, this is the first time that the size distributions of individual constituents of PIM are derived from in situ optical measurements of angular scattering. The results will contribute further to knowledge of coastal ocean biogeochemistry.

2. Materials and methods

2.1. Field experiment and measurements

The field experiment was conducted in Mobile Bay, Alabama (17–26 February 2009), which is a relatively shallow estuary system dominated by minerogenic particles from terrestrial runoff and resuspension (Fig. 1). At each sampling station, the water samples were collected at a depth of about 1.0–1.5 m for laboratory analysis of particulate matter and HPLC analysis. In addition, the volume scattering functions (VSFs) of water at about the same depth was measured by a prototype Multi-spectral Volume Scattering Meter (MVSM) at eight wavelengths and a commercial LISST-100X at 532 nm (Type B; Sequoia, Inc.). The VSFs by LISST-100X at angles from 0.07 to 9.4° and the VSFs by MVSM at 532 nm at angles from 9.5 to 179° were combined to form a complete angular resolution of the scattering (at over 600 angles between 0.07 and 179°). The combined VSFs were used in inversion to infer amorphous silica particulates and clay particulates as briefly described below. Due to the shallowness of Mobile Bay, the suspended particulates are highly dynamic when weather systems move through the bay and create significant resuspension events (Zhao et al., 2011). A cold front moved from north through Mobile Bay from 19 to 23 February 2009 (Fig. 2). On 20 and 22 February, the bay sediments were in such high concentration (up to 99 mg/L) that optical instruments were unable to take reliable measurements. The paired sample collection and reliable optical measurements are listed in Table 1. Here, we reported results from 16 sets of measurements, among which 11 were taken outside the bay at stations 1–4 and 5 inside the bay at stations 5–8.

2.2. Partitioning particulate inorganic matter

The determination of PIM is based on standard Loss-On-Ignition (LOI) detailed in Stavn and Richter (2008) so we only give a brief account here. Water samples (0.5–1.5 L) were filtered through Whatman GF/F glass fiber filters. Though rated with a 0.7 μm mean pore size, studies have shown that the GF/F filters can effectively retain particles down to 0.2 μm diameter (Chavez et al., 1995) because adsorption is the major process by which glass fiber filters remove particulate material from suspension (Johnson and Wangersky, 1985). In this study, we considered the effective pore size of the filters we used to be 0.2 μm. Filters were pre-washed, dried, and pre-weighed. Filtration was under a vacuum. Filters were dried at 103° C for 2 h, weighed, ashed at 550° C for 15 min, and weighed again. The ashing procedure was repeated until constant weight was achieved; and the final weight gives the mass of

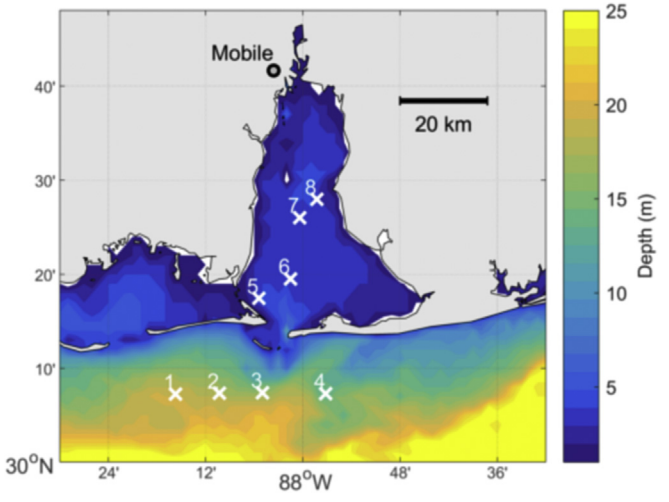

Fig. 1. The sampling stations, some of which were visited multiple times during the experiment, are overlaid over the bathymetry map. Refer to Table 1 for visiting schedule.

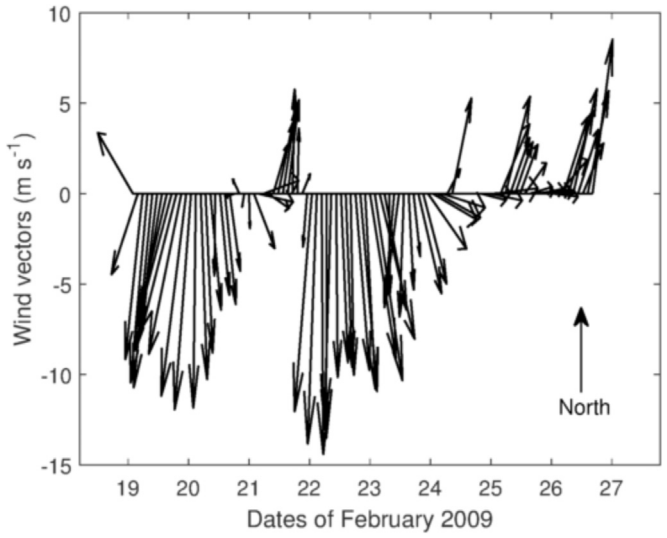

Fig. 2. The wind directions and speeds measured at the station MBLA1 (approximately at the same location as station 7 in Fig. 1) operated by Dauphin Island Sea Lab. The data were downloaded from NOAA National Data Buoy Center (http://www.ndbc.noaa.gov/).

PIM (mg L^{-1}). Before the LOI, the filters were also analyzed using an AMRAY 1820 digital SEM. The individual grains viewed on the filter were identified by energy dispersive spectral analysis (EDS), and subsequently grouped into clay species versus amorphous silica (Zhang et al., 2014). Trace amounts of clastic quartz, pyrite and TiO_2 were also found but assumed to be negligible in the total mass of PIM. Using their respective area fractions determined from the SEM images, PIM was further partitioned into a mass of clay minerals and a mass of amorphous silica.

2.3. VSF-inversion of clay and amorphous silica

The sizes, composition, shape and structure of particles affect, and hence can be potentially inferred from, the angular distribution of their VSFs. This is the theoretical basis driving the VSF-inversion (Zhang et al., 2011, 2012). The approach has been tested successfully in a series of studies in retrieving the overall particle distribution of sizes between 0.5 and 100 μm in coastal waters around the US (Zhang et al., 2012), size distribution of natural bubble populations off Hawai'i (Czerski et al., 2011) and in a surf zone off the coast of California (Twardowski et al., 2012), chlorophyll concentration in Chesapeake Bay (Zhang et al., 2013), and mass concentrations of POM and PIM in Monterey Bay and Mobile Bay (Zhang et al., 2014). Basically, a measured VSF is partitioned through a Least-squares based inversion into an optimal combination of contributions by particle subpopulations, each of which is uniquely represented by a refractive index (a surrogate for particle composition) and a log-normal size distribution (Zhang et al., 2011). Further grouping of these subpopulations by sizes and/or refractive indices would produce a particle assemblage that corresponds to natural particle populations. Zhang et al. (2014), for example, grouped sub-populations with modal sizes > 0.2 μm to resemble the particulate matter that are operationally defined based on filtration in oceanography, and among these aggregated subpopulations, they showed that those with refractive indices ≥ 1.10 correspond well to PIM and those with indices < 1.10 to POM. Here, we continued the Zhang et al. (2014) study by further refining the partition of PIM into clay minerals and amorphous silica based on the refractive index. The PIM particles (of sizes > 0.2 μm) inferred from VSF-inversion include three subpopulations represented by refractive indices = 1.10, 1.14 or 1.20. The refractive index of silica ranges 1.07–1.10 (Aas, 1996). The clay minerals typically consist of chlorite, illite, kaolinite, and montmorillonite (Griffin et al., 1968). The dominant clay minerals in the Mobile Bay system are kaolinite, montmorillonite and illite (Doyle and Sparks, 1980; Isphording and Lamb, 1979), whose refractive indices are approximately 1.16, 1.17 and 1.18, respectively (Babin et al., 2003). In this study, we assume the VSF-inversion derived PIM subpopulations with refractive index = 1.10 to be representative of amorphous silica and those with refractive indices = 1.14 or 1.20 to be representative of clay minerals.

We have followed Zhang et al. (2014) to estimate the mass concentration for each PIM species, i.e.,

$$M = \frac{4\pi}{3}\int_{0.2}^{1000}\left(\frac{d}{d_0}\right)^{F(d)} d_0^3 \rho f(d) dd \quad (1)$$

where $f(d)$ represents the size distribution inferred from the VSF-inversion, ρ is the density of PIM particles that will be estimated from the refractive index (n) as

$$\rho = \begin{matrix} 15.52(n-1) & 1.10 \le n < 1.16 \\ 6.42n - 4.86 & 1.16 \le n \end{matrix}, \quad (2)$$

$F(d)$ is the fractal dimension of the particles and assumed $F(d) = 3(d/d_0)^{-0.0533}$ following Khelifa and Hill (2006), and $d_0 = 1.0$ μm, representing the diameter of primary particles.

Table 1
Schedule of stations for the 2009 field experiment in Mobile Bay, Alabama (Fig. 1). Multiple stations are listed in the order visited on a given day. Laboratory results from water samples include gravimetric determination of mass concentrations for clay minerals and amorphous silica (partitioned using energy dispersive spectral analysis), and HPLC analysis for chlorophyll-a ([Chl]) concentration and percentage diatom fraction. VSF-inversion results include number concentrations for clay minerals and amorphous silica. Underlined values represent station 3 and bold values represent 25 February transect.

Date	19 Feb	21 Feb	23 Feb	24 Feb	25 Feb	26 Feb
Station	5	1 2 3 4	1 2 3	1 2 3	**7 6 3**	8 8
Mass concentrations from water samples						
Clay (mg/L)	3.25	0.13 1.69 1.59 0.87	0.46 1.12 0.64	0.64 1.18 0.66	**0.75 1.43 0.32**	1.03 0.81
Silica (mg/L)	2.74	0.05 0.94 0.88 0.48	0.31 0.79 0.44	0.49 0.93 0.51	**1.66 2.36 0.27**	2.71 2.12
[Chl] (μg/L)	9.56	2.27 3.52 3.72 2.73	3.08 2.96 2.83	3.06 3.24 2.97	**7.15 4.15 1.36**	14.84 15.15
Diatom (%)	83	82 76 77 82	74 78 77	73 76 77	**76 53 69**	41 42
Particle number concentrations from VSF-inversion						
Clay (× 10^{10} m^{-3})	13.94	0.32 11.32 8.89 1.03	1.13 1.88 0.27	0.09 2.02 0.37	**18.09 16.16 0.08**	7.48 12.32
Silica (× 10^{12} m^{-3})	2.20	0.50 2.00 1.43 1.10	0.57 1.27 0.70	0.61 1.00 0.63	**2.42 2.23 0.29**	2.05 2.19

2.4. Organic diatom frustule residue

The VSF-inversion uses the refractive indices for classification of different particle species. Misclassification is expected because some particles are themselves a mixture of organic and inorganic materials. Living diatom cells, for example, have a silica shell with a representative refractive index of ~1.07–1.10 (Aas, 1996), the same as detrital amorphous silica. Therefore, the mass concentration for amorphous silica estimated from the VSF-inversion (i.e., Eq. (1)) includes organic diatom frustule residue. To estimate this organic residue, cultures of diatoms were sampled in the logarithmic growth phase in which it was assumed that all amorphous silica was associated with living cells. The cultures were analyzed for total chlorophyll *a* concentration and then subjected to standard LOI analysis. The mass concentration of organic diatom frustule residue M_{ORES} (mg L^{-1}) was empirically related to the concentration of total chlorophyll *a* (μg L^{-1}) of diatoms:

$$M_{ORES} = 0.0107 + 0.00466[Chla]. \quad (3)$$

Equation (3) was derived from diatom cultures, to apply it for the field measurements it is necessary to know what percentage of the total chlorophyll concentration is contributed by diatoms, which was accomplished with the High Performance Liquid Chromatography (HPLC) data on the concentration of diagnostic pigments collected at the sampling sites (Fig. 1 and Table 1). In calculating the diatom fraction, we followed the Vidussi et al. (2001) method using fucoxanthin as a diagnostic pigment marker for diatom. The organic portion of diatom frustules estimated using Eq. (3) needs to be subtracted from the total amorphous silica mass estimated using Eq. (1).

3. Results

3.1. Analysis of water samples

The water samples were analyzed for total chlorophyll *a* concentration and fraction of diatoms from HPLC, and mass concentrations of PIM clay minerals and PIM amorphous silica (Fig. 3 and Table 1). An $R^2 = 0.61$ relationship was found in concentrations between amorphous silica and chlorophyll *a* (Fig. 3), indicating a chiefly biogenic origin for the silica minerals in Mobile Bay. The HPLC results indicated that diatoms accounted for 40–83% of the phytoplankton assemblage during the experiment (Table 1). Actually, a stronger relationship with $R^2 = 0.69$ was found between fucoxanthin and amorphous silica concentrations. A much weaker correlation was found between clay minerals and chlorophyll-a concentrations ($R^2 = 0.14$), which is expected as the major source of clay minerals in Mobile Bay is from river runoff and/or resuspension from the sediment (Sionneau et al., 2008) and is not necessarily associated with the chlorophyll distribution.

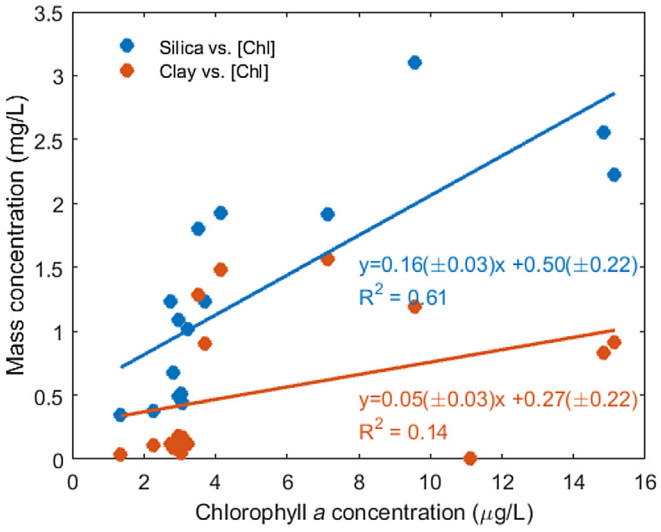

Fig. 3. Variations of mass concentrations of clay minerals and amorphous silica determined in the laboratory analysis with chlorophyll *a* concentration determined via HPLC analysis.

3.2. PIM partitions from VSF-inversion

The mass concentrations of amorphous silicate estimated from the VSF-inversion agreed very well with the laboratory determination (Fig. 4). As mentioned above, we have applied a correction (Eq. (3)) to remove the diatom frustules associated with organic residue. The effect of this correction is relatively limited; for example, the correlation coefficient, root mean square error, and mean relative error are 0.93, 0.37 mg/L and 0.21, respectively with the correction and are 0.94, 0.40 mg/L and 0.27, respectively without correction. This is mainly because diatom frustules typically contain <10% of organic matter as we found out in the laboratory experiment. The VSF-inversion method underestimated the mass concentration of clay minerals by 67% as compared to the laboratory determination, even though there was a general agreement ($R = 0.57$) between the two estimates (Fig. 4). This underestimate in clay by the VSF-inversion was, however, partially canceled out by a slight overestimate in amorphous silica, resulting in a good agreement with the total PIM, which is also consistent with the Zhang et al. (2014) results.

3.3. Particle size distributions

One unique feature of the VSF-inversion is its ability to infer the particle size distribution (PSD) associated with each particle species. The total number concentrations were estimated from the

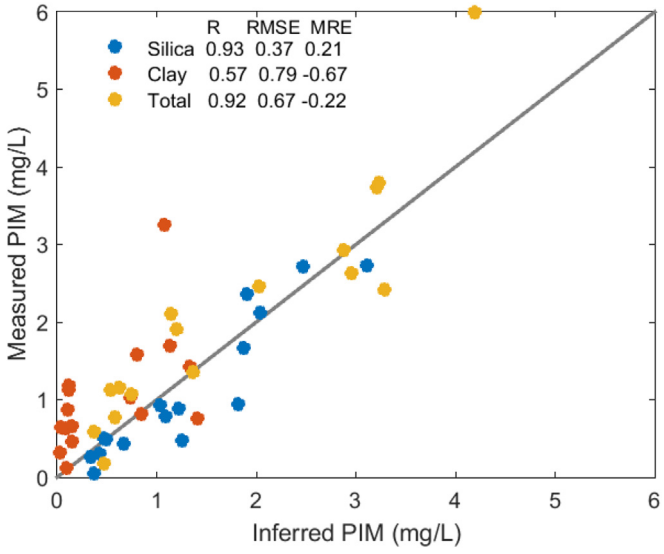

Fig. 4. Comparisons of mass concentrations of amorphous silicate, clay minerals and combined PIM by VSF-inversion and laboratory analysis. The grey line represents 1:1 relationship. The three values shown for each comparison in the legend are correlation coefficient (R), root mean square error (RMSE) and mean relative error (MRE), respectively (negative MRE indicate that the measured values exceeded the inferred values).

inferred PSDs (Table 1). The concentrations of amorphous silica, on the order of 10^{11} to 10^{13} m^{-3}, are greater than the concentrations of clay minerals, which varied between 10^{8} to 10^{12} m^{-3} with an average around 10^{10} m^{-3} (Table 1). The number concentrations of clay minerals inside the bay (stations 5, 6, 7 and 8; Fig. 1) were on average one order of magnitude higher than the concentrations outside the bay (stations 1, 2, 3 and 4); similar variations were observed for amorphous silica, even though the difference were only about 4–5 fold. Exceptions were observed for stations 2 and 3 on 21 February when the concentrations for both clay minerals and amorphous silica were comparable to the inside-bay values. The number concentrations also show a stronger correlation with chlorophyll *a* concentration for silica ($R^2 = 0.50$) than for clay minerals ($R^2 = 0.16$), consistent with the corresponding relationship shown in Fig. 3 for the mass concentrations.

We examine the general shape of size distributions in Fig. 5 by normalizing the inferred PSDs by the corresponding total number concentrations. In general, the size distributions of amorphous silica are broader than those of the clay minerals, essentially extending from less than 0.3 μm to about 100 μm with a consistent peak at about 0.8 μm and with elevated concentrations for sizes >10 μm at some stations. The size distributions of clay minerals exhibited peaks between 1 and 4 μm and saw rapid dropping in concentration at both smaller and larger sizes. On average, more amorphous silica particles of sizes >10 μm were present inside than outside the bay, whereas clay minerals exhibited a comparatively wider distribution inside than outside the bay.

A cold front with wind speeds up to 15 m s^{-1} reached the area 19–23 February, and it was relatively calm on 24 and 25 February with wind speeds <6 m s^{-1} (Fig. 2). To further examine how PIM in Mobile Bay responded to this wind event, we plotted the derived PSDs in Fig. 6 for station 3 from 21–25 February and over a transect covering stations 7, 6 and 3 on February 25. The corresponding laboratory and inversion results are underlined in Table 1 for station 3 and displayed in bold font for the transect.

Along the stations 7, 6, 3 transect (Fig. 1), there are significant differences in number concentrations for both PIM species between the inside and the outside of the bay (Table 1). The number concentrations of amorphous silica decreased from 2.2 to 2.4 × 10^{12} m^{-3} for stations 7 and 6 to about 0.3 × 10^{12} m^{-3} for station 3 (Table 1). Much more dramatic decrease was found for clay minerals, from about 16–18 × 10^{10} m^{-3} at stations 7 and 6 to only 0.08 × 10^{10} m^{-3} at station 3. Accompanying the decrease in the number concentration, clay minerals exhibited two major changes in size distribution (Fig. 6-b). The overall PSDs became narrower in shape and the location of the dominant peak changed from ~2 μm at stations 7 and 6 to ~4 μm at station 3. For amorphous silica, the overall PSDs were similar with a peak around 0.8 μm, and most of the changes in PSDs were for sizes >4 μm with no clear pattern along the transect (Fig. 6-d). For example, station 3 had higher concentration of amorphous silica of sizes between 4 and 10 μm and station 6 had more amorphous silica at sizes >10 μm.

During and after the cold front from 21 to 25 February, the retrieved number concentrations at station 3 were 8.89, 0.27, 0.37, and 0.08 × 10^{10} m^{-3} for clay minerals; 1.43, 0.70, 0.63, and 0.29 × 10^{12} m^{-3} for amorphous silica (Table 1). Accompanying this decrease in total number concentrations, clay minerals changed from bi-modal distributions on 21 and 23 February with peaks at approximately 2 and 4 μm to unimodal distributions on 24 and 25 February with a peak at 4 μm (Fig. 6-a). Similar to the transect case, the size distribution of amorphous silica remained roughly the same with most of the changes occurring at sizes >4 μm (Fig. 6-c). The PSDs inferred for amorphous silica at station 3 were very similar to each other on 21 and 25 February when south winds with speeds <6 m s^{-1} were observed (Fig. 2), both had a shoulder between 4 and 10 μm. On 23 February with a strong north wind of speeds up to 12 m s^{-1}, the PSD at station 3 was similar to that of station 6, both having significant presence of amorphous silica of sizes >10 μm. On 25 February when the cold front died down, amorphous silica showed the narrowest PSD.

3.4. Phase functions

The VSF-inversion is based on the fact that particles of different types and size distributions exhibit distinctive angular scattering patterns, i.e., the phase functions. The average phase functions estimated from the inversion for amorphous silica and clay minerals differ considerably (Fig. 7). At angles <1°, scattering by amorphous silica continued increasing while that by clay minerals leveled out. Relative to clay minerals, amorphous silica also exhibited elevated scattering at angles between 15 and 60°, and at angles >90°. On average, the phase function shape for either

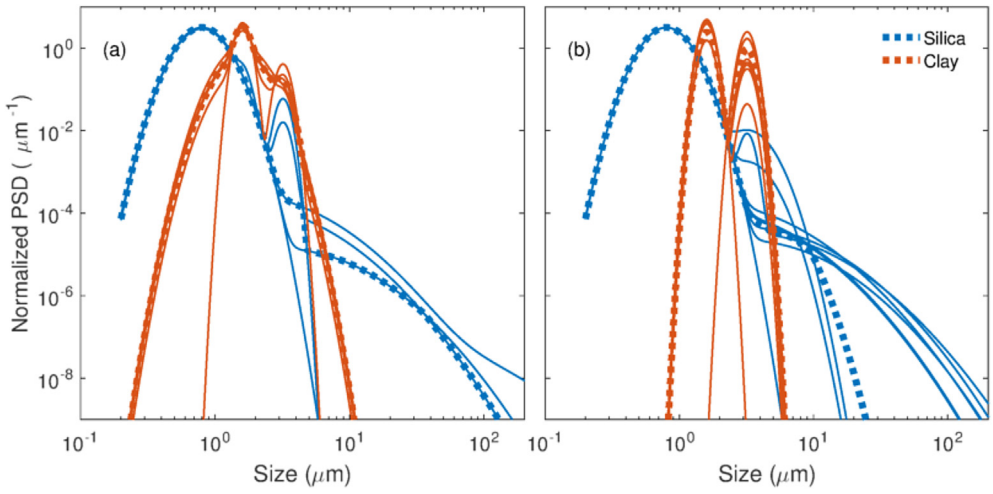

Fig. 5. Particle size distributions normalized by the corresponding number concentrations for inside (a) and outside (b) the bay. Blue curves are for amorphous silica and red ones for clay minerals. Solid lines represent the inversion-derived results for each individual measurement and the thick dotted lines represent the median size distributions. (For interpretation of the references to colour in this figure legend, the reader is referred to the web version of this article.)

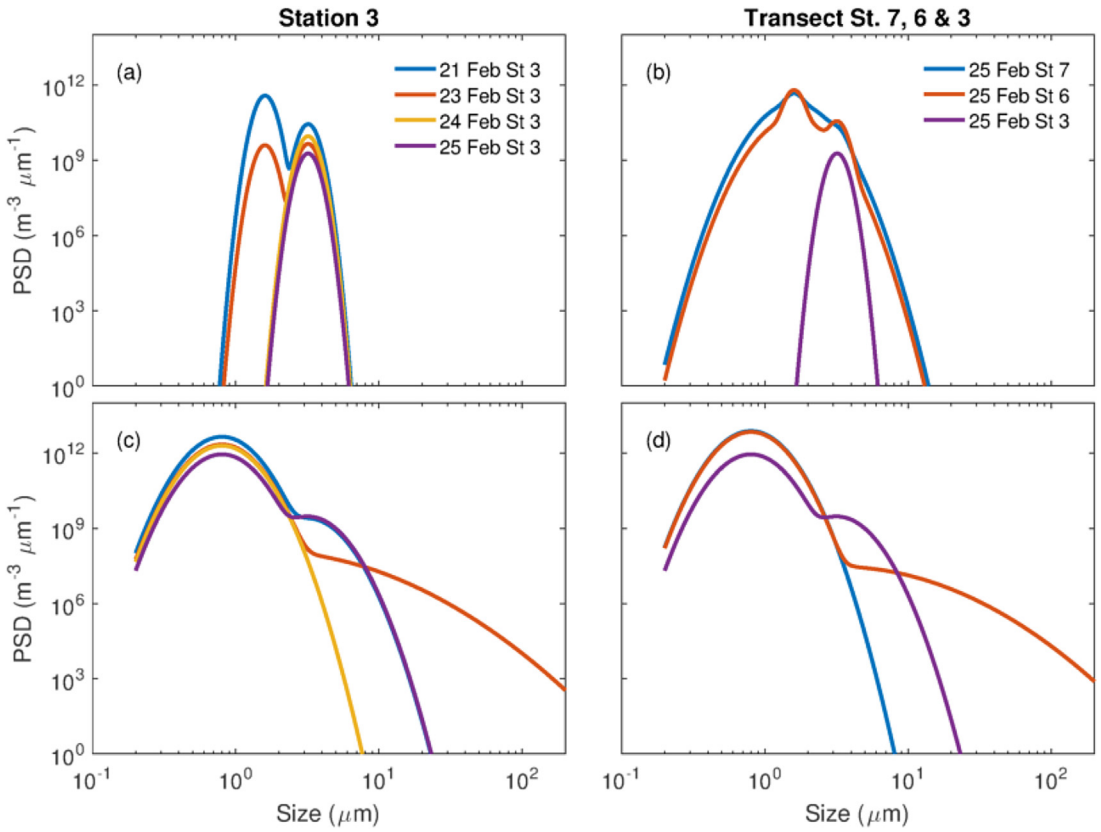

Fig. 6. Particle size distributions for clay minerals (a and b) and for amorphous silica (c and d) as inferred from the measured VSFs at station 3 on 21, 23, 24 and 25 February (left column) and along a transect covering stations 7, 6 and 3 on 25 February 25, 2009 (right column).

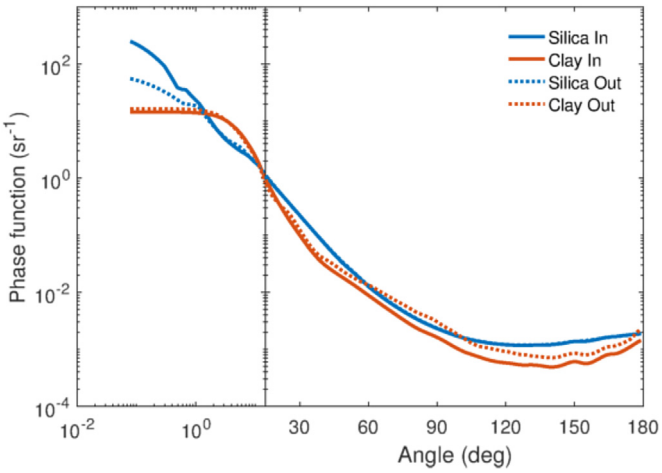

Fig. 7. The average phase functions estimated from the inversion for amorphous silica and clay minerals inside and outside the bay. To better depict the changes of phase functions at near forward angles, the x-axis is in logarithmic scale for angles <15°.

amorphous silica or clay minerals was similar between inside and outside the bay, with small but observable difference at angles <1° for amorphous silica and at angles >60° for clay minerals.

4. Discussion

A major advantage of the VSF-inversion technique is the ability to separate amorphous silica and clay minerals from each other and examine their particle dynamics separately. Since the separation is based on the refractive index, particles different from but of similar refractive indices to amorphous silica (or clay minerals) would be classified into the amorphous silica (or clay minerals) group. This potential misclassification is an uncertainty associated with this method because particles of similar refractive index (and sizes) would scatter light similarly. In other words, different particles of the same refractive index cannot be separated solely based on the scattering of light. In this study, we assigned a refractive index of 1.10 to represent amorphous silica and refractive indices of 1.14 and 1.20 to represent clay minerals. The results shown in Fig. 4 indicate the method has been able to identify and quantify amorphous silica reasonably well but underestimate the mass for clay minerals, which may include some particle species that were identified as clay minerals by energy dispersive spectral analysis but cannot be optically represented by the two refractive indices (1.14 and 1.20) used in this study. For example, among clay minerals and diatom frustules, trace amounts of titanium oxide, pyrite and clastic quartz were also found in the water samples (see Fig. 2 in Zhang et al., 2014). These trace minerals were included in the mass of clay minerals, but will not be represented by our inversion method because we have assumed the upper bound of refractive index for major aquatic particles is 1.22 (Aas, 1996) whereas the relative refractive indices of TiO_2 and pyrite are ~ 2.0 and ~1.3, respectively. Also, TiO_2 and pyrite are much heavier ($\rho \approx 4.0$ and 4.8 g cm^3) than kaolinite, montmorillonite and illite ($\rho \approx 2.5$–2.9 g cm^3), the three dominant clay minerals in the Mobile Bay system. Therefore, our inversion results for clay minerals should be interpreted as representing only those mineral species whose refractive indices are within 1.12–1.22 (Zhang et al., 2011).

The phase function of a natural particle population in the ocean is largely determined by its composition and size distribution (Zhang et al., 2011). Generally speaking, the presence of large

particles (relative to the wavelength of the incident light, 532 nm here) would enhance the scattering at the near forward angles whereas the presence of small particles enhances the scattering at relatively larger angles, particularly at backward angles (>90°), which would also increase with the refractive index of particles (Bohren and Huffman, 1983). Compared to clay minerals, significant amounts of amorphous silica existed in Mobile Bay with sizes >10 μm and <1 μm (Fig. 5), which led to their elevated scattering at angles <1° and >90°, respectively (Fig. 7). Amorphous silica has a lower refractive index, and hence is expected to exhibit less backscattering, than clay minerals if the two species have the same size distribution. However, because the differences between their respective refractive index values are relatively small (1.10 vs. 1.04 and 1.20), the greater concentrations of submicron amorphous silica found in Mobile Bay (Fig. 5) has more than compensated for its relatively weaker refractivity.

While collectively recognized as the particulate inorganic matter, amorphous silica and clay minerals, as shown in this study, possess very different size distributions (Fig. 5), reflecting the interaction of biogeochemical and physical processes that control particle dynamics in the area. To our knowledge no independent estimates exist, so we do not know the uncertainty of inferred size distributions for these mineral species. However, the bulk particle distributions estimated using our method for sizes 1–200 μm have been shown to agree with the determination using the Laser diffraction method (LISST-100X by Sequoia Inc.) within 10% (Zhang et al., 2012). Relatively few results have been reported for PSDs in the submicron range but our results do appear to confirm the results of Atteia et al. (1998), Gallegos and Menzel (1987) and Peng and Effler (2007) in which submicron or colloidal distributions of minerogenic matter level off in the submicron range and do decrease at the smallest sizes in a couple of cases where the measurement technique extended far enough into the submicron range.

Sionneau et al. (2008) discussed three processes that largely control the distribution of particles of the Northern Gulf of Mexico: particle sources, settling and advection. Over a shallow estuarine environment, such as Mobile Bay, wind-induced sediment suspension could also significantly alter the distribution of particles (Walker, 2001; Walker and Adele, 2000; Zhao et al., 2011). Since the duration of the experiment coincided with the passage of a cold front, we believe all four factors came into play in controlling and modifying the particle dynamics of amorphous silica and clay minerals in Mobile Bay.

The February–March period in Mobile Bay is the time of the spring bloom, dominated by diatoms in the early stages. The HPLC analysis showed significant amounts of fucoxanthin (dominant biomarker for diatoms) in the samples, indicating that the majority of the chlorophyll detected was due to the presence of diatoms (Table 1). Therefore, the major source of amorphous silica in the area is from blooming diatoms, also consistent with the high correlation observed between the concentrations of amorphous silicate and chlorophyll (Fig. 3). Because amorphous silica is mainly autochthonous, the size distributions (Fig. 5) are nearly identical to each other from 0.2 to 4 μm with a dominant peak around 0.8 μm, which could represent frustule residues of smaller diatom species or fragments of larger frustules generated by zooplankton consumption. The tail at larger sizes could be associated with two possible sources. The first could be due to more intact detrital frustules added to the water body by production of some larger diatom species in the bloom, which could explain the intermittent pattern of the appearance of larger sizes at the various sampling stations. Kranck and Milligan (1988), following the course of a diatom bloom in Bedford Basin, Nova Scotia, reported that the individual cells of the bloom remained small and intact but after nutrient depletion and death of the cells that the frustules became attached and formed relatively large aggregates. So the second source could be the aggregate formation at the end of a bloom. Thus we have summations of possibly separate particle populations of amorphous silica yielding PSDs as shown in Fig. 5.

In contrast to autochthonous amorphous silica, clay minerals are primarily allochthonous from river runoff (Griffin et al., 1968). In Mobile Bay, the major components of clay minerals are montmorillonite, kaolinite and illite (Isphording and Lamb, 1979; Milne and Earley, 1958). Using five experimental techniques – electro-optical birefringence, ultracentrifugation, viscometry, optical transmission and electron microscopy, Kahn (1959) determined the average sizes of clay particles in aqueous suspension are 0.5–2.5 μm for montmorillonite and 0.3–0.8 μm for illites. Arnott (1965) measured dry powdered clay sizes using small-angle X-ray scattering; assuming approximately 0.3 μm swelling in water suspension (West, 1952), we estimated that the average sizes are 0.75–1.2 μm for montmorillonites and 0.6–0.9 μm for illites, agreeing well with the measurements of Kahn (1959). Johnson and Kelley (1984) conducted the mineralogical analysis of Mississippi river suspended sediment and found that these three mineral species account for all the suspended sediment of sizes < 2 μm and only kaolinite is found at sizes of 2–7.8 μm but only accounting for < 20% of particles. Assuming the Johnson and Kelley (1984) conclusion applies to Mobile Bay, we would then expect the sizes of clay minerals in Mobile Bay be mainly confined to sizes < 2 μm, which is generally consistent with Fig. 5 showing that the clay minerals have peaks between 1 and 4 μm.

Settling of particles in the aquatic environment (e.g., Chase, 1979) depends on both particle characteristics and environmental condition as well as their interaction (e.g., Camenen, 2007). In any given environment, the larger or denser particles would settle faster. The density of silica is ~1.9×10^3 kg m^{-3}, while densities of clay minerals are approximately $2.0–2.5 \times 10^3$ kg m^{-3}, $2.60–2.65 \times 10^3$ kg m^{-3}, and $2.80–2.85 \times 10^3$ kg m^{-3} for montmorillonite, kaolinite and illite, respectively (Babin et al., 2003; Wozniak and Stramski, 2004). Suspended clay minerals, upon entering saline waters, become ionized, flocculate, or aggregate together, and settle out more rapidly than they would as single particles (Isphording and Lamb, 1979). Among clay minerals, kaolinite and illite flocculate and settle faster than montmorillonite which flocculate slowly (Porrenga, 1966) and in northern coast of Gulf of Mexico, illite floccules, though smaller, settle more rapidly due to their higher density (Sionneau et al., 2008).

Booth et al. (2000) developed an empirical model of sediment resuspension in shallow estuaries as a function of water depth, wind speed, direction and fetch based on surface gravity wave theory and validated the model for the Barataria Basin, Louisiana, USA. Applying this model, we estimated that critical wind speeds for sediment resuspension inside Mobile Bay (water depth = 5 m; fetch = 10–20 km) are 3.5–5.5 m s^{-1}, and about 11 m s^{-1} outside the Bay (water depth = 25 m; fetch = 50 km). During the experiment, nearly 90% of the time winds had a speed >3.5 m s^{-1}, inducing resuspension inside the bay. Even though wind speeds reached over 11 m s^{-1} during the cold front (Fig. 2), because the winds were from the north, the fetch, and hence sediment resuspension, was limited at stations 1–4 outside the bay. Zhao et al. (2011) conducted a 3-D hydrodynamic simulation on particle movement in Mobile Bay and found that approximately 10% of suspended particles would be flushed out through the exit of the barrier islands during a cold front. Therefore, we would expect sediment resuspension had occurred nearly continuously inside the bay (stations 5–8) but seldom outside the bay (stations 1–4) during the period of the experiment. However, stations outside the bay, particularly station 3 which is located immediately south of the exit of the barrier islands (Fig. 1), would be impacted by suspended

particulates transported out of the bay by a strong northerly wind.

Because of lower density and hence lower settling-speed, amorphous silica exhibits a broader size distribution than clay minerals (Fig. 5). The elevated concentrations inferred for amorphous silica of sizes >10 μm inside the bay (Fig. 5-a) are probably due to wind-induced resuspension. As clay minerals are being transported away from the river mouth, the rapid settling of larger minerals and denser (probably smaller) illites could lead to a size distribution that becomes narrower from inside (red curves in Fig. 5-a) to outside (red curves in Fig. 5-b) the bay. Inside the bay, however, the nearly constant wind-induced resuspension during the experiment would lift those settled clay minerals back into the water body, which explains that the inferred concentrations of clay minerals were relatively similar at stations 7 and 6 but dropped by a factor of 200 at station 3 (Table 1). It is also interesting to note that smaller clay minerals of sizes <2 μm accounted for most of the concentration reduction (Fig. 6-b). As mentioned above, illites are of smaller sizes (Kahn, 1959) but greater density (Babin et al., 2003; Wozniak and Stramski, 2004) among the three clay mineral species that enter Mobile Bay and tend to settle faster than the others (Sionneau et al., 2008). We hypothesize that the differential settling of smaller illite contributes to the disappearance of submicron clay minerals between stations 7 and 6 and station 3 (Fig. 6-b).

During the cold front, suspended particles would be flushed out from the bay through the barrier island exit (Zhao et al., 2011). Both clay minerals and amorphous silica at station 3 showed elevated concentrations on 21 February, which subsequently decreased as the cold front passed (underlined values in Table 1). The flushed-out clay minerals, probably consisting of a significant amount of resuspended illites, contributed to the appearance of a smaller peak in the PSDs of size about 2 μm on 21 and 23 February at station 3 (Fig. 6-a). As these smaller yet denser illites settled out of the surface layer in the following two days, the clay minerals returned to a unimodal distribution with a peak at 4 μm on 25 February (Fig. 6-a).

The estimated diatom fractions at station 3 were 77% on 21, 23 and 24 and dropped slightly to 69% on 25 February (Table 1). Therefore, the initial increase of amorphous silica at station 3 during the cold front was mainly due to advection from inside the bay. Note the similarity of amorphous silica PSDs between station 3 and station 6 (Fig. 6-d). This advection also contributed to the elevated concentrations of amorphous silica of sizes >10 μm observed on 23 February (Fig. 6-c). The settling of these larger amorphous silica would return the PSD to a shape on 25 February that is similar to that on 21 February (Fig. 6-c).

5. Conclusions

The angular pattern of scattered light contains detailed information about the size and composition of particles (Bohren and Huffman, 1983). Continuing from our earlier studies (Zhang et al., 2011, 2012, 2013, 2014), we determined the PSDs and associated quantitative relations of major components of suspended mineral matter (PIM), amorphous silica and clay minerals, from measured volume scattering functions in Mobile Bay. The PSDs of autochthonous amorphous silica exhibit two unique features: a broad peak centered at about 0.8 μm for sizes between 0.2 and 4 μm and a very broad shoulder essentially extending from 4 μm to >100 μm. With an active and steady particle source from blooming diatoms, the shapes of amorphous silica PSDs for sizes <10 μm varied little across the stations, but showed more particles of sizes >10 μm inside the bay, likely due to wind-induced resuspension of larger frustules that have settled. Compared to amorphous silica, the allochthonous, clay minerals are denser and exhibit relatively narrower PSDs with peaks located between 1 and 4 μm. Preferential settling of larger mineral particles as well as smaller but denser illite component further narrowed down the size distributions of clay minerals as they are being transported outside the bay. The derived PSDs also indicated a very dynamic situation in Mobile Bay relative to the weather front that passed through. During the cold front, both amorphous silica and clay minerals showed a dramatic increase in concentration and broadening in size distribution at station 3, located south of the exit of the barrier islands, indicative of wind-induced resuspension and subsequent advection of particles out of Mobile Bay (Zhao et al., 2011). The results also demonstrate the potential of applying VSF-inversion in studying biogeochemistry in the estuarine-coastal ocean system.

Acknowledgements

Sonia Gallegos collected and filtered the water samples from Mobile Bay. She is in the Bio-optical Physical Processes & Remote Sensing Section, Code 7331, Naval Research Laboratory, Stennis Space Center, MS. DJG and RWG were supported by the NRL projects: Determining all Intrinsic Optical Properties of Coastal Waters with an Off-nadir Airborne Hyperspectral Sensor; Bio-optical Studies of Predictability and Assimilation for the Coastal Environment. RHS was supported by Naval Research Laboratory project: Predicting Coastal Bio-optical Response to Atmospheric/Oceanographic Forcing, to RWG. XZ is supported by funding from National Science Foundation 1458962 and 1355466, and from National Aeronautics and Space Administration NNX13AN72G and NNX15AC85G.

References

Aas, E., 1996. Refractive index of phytoplankton derived from its metabolite composition. J. Plankton Res. 18, 2223–2249.
Arnott, R.J., 1965. Particle sizes of clay minerals by small-angle X-ray scattering. Am. Miner. 50, 1563–1575.
Atteia, O., Perret, D., Adatte, T., Kozel, R., Rossi, P., 1998. Characterization of natural colloids from a river and spring in a karstic basin. Environ. Geol. 34, 257–269.
Babin, M., Morel, A., Fournier-Sicre, V., Fell, F., Stramski, D., 2003. Light scattering properties of marine particles in coastal and open ocean waters as related to the particle mass concentration. Limnol. Oceanogr. 48, 843–859.
Bohren, C.F., Huffman, D.R., 1983. Absorption and Scattering of Light by Small Particles. John Wiley & Sons, New York.
Booth, J.G., Miller, R.L., McKee, B.A., Leathers, R.A., 2000. Wind-induced bottom sediment resuspension in a microtidal coastal environment. Cont. Shelf Res. 20, 785–806.
Bowers, D.G., Binding, C.E., 2006. The optical properties of mineral suspended particles: a review and synthesis. Estuar. Coast. Shelf Sci. 67, 219–230.
Camenen, B., 2007. Simple and general formula for the settling velocity of particles. J. Hydraul. Eng. 133, 229–233.
Chase, R.R.P., 1979. Settling behavior of natural aquatic particulates1. Limnol. Oceanogr. 24, 417–426.
Chavez, F.P., Buck, K.R., Bidigare, R.R., Karl, D.M., Hebel, D., Latasa, M., Campbell, L., Newton, J., 1995. On the chlorophyll a retention properties of glass-fiber GF/F filters. Limnol. Oceanogr. 40, 428–433.
Corbett, D.R., McKee, B., Duncan, D., 2004. An evaluation of mobile mud dynamics in the Mississippi River deltaic region. Mar. Geol. 209, 91–112.
Czerski, H., Twardowski, M., Zhang, X., Vagle, S., 2011. Resolving size distributions of bubbles with radii less than 30 μm with optical and acoustical methods. J. Geophys. Res. 116, C00H11.
DeMaster, D.J., 1981. The supply and accumulation of silica in the marine environment. Geochim. Cosmochim. Acta 45, 1715–1732.
Doyle, L.J., Sparks, T.N., 1980. Sediments of the Mississippi, Alabama, and Florida (MAFLA)) continental shelf. J. Sediment. Res. 50, 905–915.
Duarte, C.M., Agustí, S., Satta, M.P., Vaqué, D., 1998. Partitioning particulate light absorption: a budget for a Mediterranean bay. Limnol. Oceanogr. 43, 236–244.
Effler, S.W., Prestigiacomo, A.R., Peng, F., Gelda, R., Matthews, D.A., 2014. Partitioning the contributions of minerogenic particles and bioseston to particulate phosphorus and turbidity. Inland Waters 4, 179–192.
Fachini, A., Vasconcelos, T.M., 2005. Enhancing diatom growth by using zeolites to change seawater composition (4 pp). Environ. Sci. Pollut. Res. 13, 238–241.
Gallegos, C.L., Menzel, R.G., 1987. Submicron size distributions of inorganic suspended solids in turbid waters by photon correlation spectroscopy. Water Resour. Res. 23, 596–602.
Griffin, J.J., Windom, H., Goldberg, E.D., 1968. The distribution of clay minerals in the World Ocean. Deep Sea Res. 15, 433–459.
Howarth, R., Chan, F., Conley, D.J., Garnier, J., Doney, S.C., Marino, R., Billen, G., 2011.

Coupled biogeochemical cycles: eutrophication and hypoxia in temperate estuaries and coastal marine ecosystems. Front. Ecol. Environ. 9, 18–26.
Isphording, W.C., Lamb, G.M., 1979. The Sediments of Mobile Bay: a Report the Alabama Coastal Area Board. Dauphin Island Sea Lab, Dauphin Island, Alabama, p. 35.
Johnson, A.G., Kelley, J.T., 1984. Temporal, spatial, and textural variation in the mineralogy of Mississippi River suspended sediment. J. Sediment. Res. 54, 67–72.
Johnson, B.D., Wangersky, P.J., 1985. Seawater filtration: particle flow and impaction considerations. Limnol. Oceanogr. 30, 966–971.
Johnson, K.S., Chavez, F.P., Friederich, G.E., 1999. Continental-shelf sediment as a primary source of iron for coastal phytoplankton. Nature 398, 697–700.
Kahn, A., 1959. Studies on the size and shape of clay particles in aqueous suspension. In: Ingerson, E. (Ed.), Clays and Clay Minerals: Proceedings of the Sixth National Conference on Clays and Clay Minerals (International Series of Monographs on Earth Sciences, Volume 2). Pergamon Press, pp. 220–236.
Khelifa, A., Hill, P.S., 2006. Models for effective density and settling velocity of flocs. J. Hydraul. Res. 44, 390–401.
Kranck, K., Milligan, T.G., 1988. Macroflocs from diatoms: in situ photography of particles in Bedford Basin, Nova Scotia. Mar. Ecol. - Prog. Ser. 44, 183–189.
Le Pape, P., Ayrault, S., Quantin, C., 2012. Trace element behavior and partition versus urbanization gradient in an urban river (Orge River, France). J. Hydrol. 472–473, 99–110.
Liang, L., Luo, L., Zhang, S., 2011. Adsorption and desorption of humic and fulvic acids on SiO2 particles at nano- and micro-scales. Colloids Surf. A Physicochem. Eng. Asp. 384, 126–130.
Milne, I.H., Earley, J.W., 1958. Effect of source and environment on clay minerals. Bull. Am. Assoc. Pet. Geol. 42, 328–338.
Peng, F., Effler, S.W., 2007. Suspended minerogenic particles in a reservoir: light-scattering features from individual particle analysis. Limnol. Oceanogr. 52, 204–216.
Porrenga, D.H., 1966. Clay minerals in recent sediments of the Niger Delta. Clays Clay Miner. 14, 221–233.
Risović, D., 1993. Two-component model of sea particle size distribution. Deep Sea Res. Part I Oceanogr. Res. Pap. 40, 1459–1473.
Salomons, W., Mook, W.G., 1977. Trace metal concentrations in estuarine sediments: mobilization, mixing or precipitation. Neth. J. Sea Res. 11, 119–129.
Schlegel, M.L., Manceau, A., Charlet, L., Chateigner, D., Hazemann, J.-L., 2001. Sorption of metal ions on clay minerals. III. Nucleation and epitaxial growth of Zn phyllosilicate on the edges of hectorite. Geochim. Cosmochim. Acta 65, 4155–4170.
Schmitt, D., Müller, A., Csögör, Z., Frimmel, F.H., Posten, C., 2001. The adsorption kinetics of metal ions onto different microalgae and siliceous earth. Water Res. 35, 779–785.
Sionneau, T., Bout-Roumazeilles, V., Biscaye, P.E., Van Vliet-Lanoe, B., Bory, A., 2008. Clay mineral distributions in and around the Mississippi River watershed and Northern Gulf of Mexico: sources and transport patterns. Quat. Sci. Rev. 27, 1740–1751.
Stavn, R.H., Richter, S.J., 2008. Biogeo-optics: particle optical properties and the partitioning of the spectral scattering coefficient of ocean waters. Appl. Opt. 47, 2660–2679.
Tombácz, E., Libor, Z., Illés, E., Majzik, A., Klumpp, E., 2004. The role of reactive surface sites and complexation by humic acids in the interaction of clay mineral and iron oxide particles. Org. Geochem. 35, 257–267.
Tréguer, P., Nelson, D.M., Van Bennekom, A.J., DeMaster, D.J., Leynaert, A., Quéguiner, B., 1995. The silica balance in the world ocean: a reestimate. Science 268, 375–379.
Twardowski, M., Zhang, X., Vagle, S., Sullivan, J., Freeman, S., Czerski, H., You, Y., Bi, L., Kattawar, G., 2012. The optical volume scattering function in a surf zone inverted to derive sediment and bubble particle subpopulations. J. Geophys. Res. 117, C00H17.
Ussher, S.J., Achterberg, E.P., Powell, C., Baker, A.R., Jickells, T.D., Torres, R., Worsfold, P.J., 2013. Impact of atmospheric deposition on the contrasting iron biogeochemistry of the North and South Atlantic Ocean. Glob. Biogeochem. Cycles 27, 1096–1107.
van der Weijden, R.D., Meima, J., Comans, R.N.J., 1997. Sorption and sorption reversibility of cadmium on calcite in the presence of phosphate and sulfate. Mar. Chem. 57, 119–132.
Vidussi, F., Claustre, H., Manca, B.B., Luchetta, A., Marty, J.-C., 2001. Phytoplankton pigment distribution in relation to upper thermocline circulation in the eastern Mediterranean Sea during winter. J. Geophys. Res. Oceans 106, 19939–19956.
Walker, N.D., 2001. Tropical storm and hurricane wind effects on water level, salinity, and sediment transport in the river-Influenced Atchafalaya-Vermilion bay system, Louisiana, USA. Estuaries 24, 498–508.
Walker, N.D., Adele, B.H., 2000. Impacts of winter storms on circulation and sediment transport: Atchafalaya-Vermilion bay region, Louisiana, U.S.A. J. Coast. Res. 16, 996–1010.
Warren, L.A., Zimmerman, A.P., 1994. The importance of surface area in metal sorption by oxides and organic matter in a heterogeneous natural sediment. Appl. Geochem. 9, 245–254.
West, W.J., 1952. Size determinations of clay particles in water suspensions by use of low-angle x-ray diffraction. J. Colloid Sci. 7, 295–305.
Wozniak, S.B., Stramski, D., 2004. Modeling the optical properties of mineral particles suspended in seawater and their influence on ocean reflectance and chlorophyll estimation from Remote sensing algorithms. Appl. Opt. 43, 3489–3503.
Zhang, X., Twardowski, M., Lewis, M., 2011. Retrieving composition and sizes of oceanic particle subpopulations from the volume scattering function. Appl. Opt. 50, 1240–1259.
Zhang, X., Gray, D., Huot, Y., You, Y., Bi, L., 2012. Comparison of optically derived particle size distributions: scattering over the full angular range versus diffraction at near forward angles. Appl. Opt. 51, 5085–5099.
Zhang, X., Huot, Y., Gray, D.J., Weidemann, A., Rhea, W.J., 2013. Biogeochemical origins of particles obtained from the inversion of the volume scattering function and spectral absorption in coastal waters. Biogeosciences 10, 6029–6043.
Zhang, X., Stavn, R.H., Falster, A.U., Gray, D., Gould Jr., R.W., 2014. New insight into particulate mineral and organic matter in coastal ocean waters through optical inversion. Estuarine, Coast. Shelf Sci. 149, 1–12.
Zhao, H., Chen, Q., Walker, N.D., Zheng, Q., MacIntyre, H.L., 2011. A study of sediment transport in a shallow estuary using MODIS imagery and particle tracking simulation. Int. J. Remote Sens. 32, 6653–6671.